

Design of a one-dimensional flexible structure for desired load-bearing capability and axial displacement

Shounak Bhattacharya,

Author,

Graduate Student, Department of Mechanical Engineering, Indian Institute of Science,
Bangalore, India.

Email: bhsapiens91@gmail.com

G.K. AnanthaSuresh,

Professor, Department of Mechanical Engineering, Indian Institute of Science, Bangalore, India.

Email: suresh@iisc.ac.in

Ashitava Ghosal,

Corresponding Author,

Professor, Department of Mechanical Engineering, Indian Institute of Science, Bangalore, India.

Email: asitava@iisc.ac.in

Abstract

A flexible spine is capable of bearing both transverse and axial external loads. At the same time, it is observed in animals that the spine deforms substantially during their motion and this allows the body to move efficiently and achieve high speeds. This paper deals with the modeling and design of one-dimensional flexible objects for a desired load-carrying capability and axial deflection. The flexible one-dimensional object is modeled as a serial chain of rigid segments connected by one-degree-of-freedom rotary joints with torsional springs and dampers at the joints. For a desired transverse and axial loading, optimization techniques are used to obtain the values of the orientation of the rigid segments, the joint stiffness and damping, which gives the desired axial displacement and the shape. It is shown that changing the orientation or the shape of the one-dimensional structure has more effect than changing the stiffness at the joints. Various types of loading and axial deflections are considered and the optimization procedure is illustrated through numerical examples. The response of such a flexible structure to a transient periodic loading is also obtained.

Keywords: Flexible multi-body system, Optimization, Articulated spine, Static and dynamic loading, Desired shape

1 Introduction

Quadruped robots are one of the key topics of interest in the field of robotics. This is motivated by four-legged animals which can carry large loads on their back and also navigate through rough terrains which are inaccessible to wheeled mobile robots. Several such legged robots have been designed and built (for example, HyQ2Max (Semini et al., 2011), ANYmal (Hutter et al., 2016), Big-dog (Raibert et al., 2008)). They mimic the motion of quadruped animals. Most of these robots have a rigid central structure along its primary axis, which reduces the flexibility of their body. The lack of flexibility reduces maneuverability and stride length. Motivated by Nature, recently researchers have attempted to design an articulated spine for a quadruped robot and this has shown encouraging results, in terms of energy efficiency and average running speed (see, for example, the MIT Cheetah (Seok et al., 2013), Bobcat (Khoramshahi et al., 2013)). These designs can be classified into two broad categories, namely, active actuated spine (Culha, 2012) and passive flexible spine (Cao & Poulakakis, 2013). In recent work, researchers (Lei, Yu, & Wang, 2016) have also studied a bionic flexible body for side-wise bending.

The spine or the vertebrae column in an animal is a flexible multi-body structure with multiple degrees of freedom (DoF) at each joint. These joints are actuated and constrained by many muscles and tendons leading to a limited motion of the spine. A one-dimensional serial chain connected by more than three joints, moving in a plane, can be thought of as a hyper-redundant serial manipulator (Chirikjian & Burdick, 1994). If the end of such a hyper-redundant serial robot is given a desired displacement, then there exists an infinite number of solutions for the joint variables to achieve the end displacement. To find a unique solution, also called the resolution of redundancy (Conkur & Buckingham, 1997), there exists several approaches. All these approaches deal with position and/or velocity of the rigid segment and not with the response to an external loading. In the statics of serial manipulators or a hyper-redundant manipulator, the issue of redundancy does not arise. For a given external force and/or moment applied at the end-effector, the reaction torques or the applied torque at the joints can be obtained from the transpose of the manipulator's Jacobian matrix (Ghosal, 2006). However, for a given prescribed end-effector motion together with external loading at the joints or at the end, the joint torques cannot be obtained uniquely for a hyper-redundant manipulator. This is because the Jacobian depends on the configuration of the manipulator that is to be determined.

The spine under external loading can be treated as a loaded multi-body serial manipulator with a constrained end-point motion. The equations of motion of a serial manipulator, redundant or otherwise, can be formulated and solved numerically. From this formulation, for a given torque at the joints, the motion of the links can be obtained and likewise the torque at the joints can be computed for a desired motion of the links. In our one-dimensional model, the muscles and tendons of the original spine are approximated by torsional springs rather than actuators. As none of the joints are active, with the introduction of torsional springs at the joints, the hyper redundant manipulator problem becomes a problem of an under-actuated system (Seifried, 2014). Obtaining the desired motion of an under-actuated serial robot and its shape, when subjected to transverse and axial loading, is much more difficult. In the case of a flexible spine, the model contains a large number of rigid segments to obtain realistic motion. As we do not introduce any actuators capable of directly controlling the states of the system, it can be described as an articulated passive system. The primary reason for this effort, when compared with a spine of a single rigid segment, is that the flexible central structure is known to be more energy efficient (Alexander, 1988). It also known to enable a higher average speed as compared to a rigid central frame. Work done by

Khormoashiha and Ijspeert (Khoramshahi et al., 2013) shows the benefits of an active spine. It is clear from this work that the larger the spine deflection, the better the average gait speed.

Obtaining the shape of a flexible structure subjected to loading or an end-point displacement and or force is also dealt in the context of shape optimization in compliant mechanisms (see, for example, the work by Xu and Ananthasuresh(2003) and the references contained therein). In these studies, the flexible links are modeled as continuous beams and a finite element formulation is used to determine the shape of the structure against external loading and desired deflection. In reference Xu & Ananthasuresh (2003) the parameters of Bezier curve have been used as the design variables. A modified version of the work has been done by Zhou and Ting (2008) where they have used wide curves to take into account the variable width-profile of the beams. In the case of the spine, the assumption of discrete rigid segments connected by joints is more reasonable and the motion of the rigid segments and the rotations at the joints can be large resulting in significant change in their orientation.

In this paper, we focus on modeling and design of flexible spines that can bear transverse loads on its axis and also deform in a desired manner due to a load applied along the axial direction. We have used the equation of motion to study the motion of a serial chain of rigid segments connected by joints with torsional springs and damping at the joints. The theory developed is applicable to an arbitrary number of segments. We assume reasonable constraints on the angular motion at the joints. For a given transverse loading, the spring stiffness and link orientation at the joints are obtained by optimizing an appropriate objective functions related to the work done by the loads. Next, for a desired end-point motion, we use a modified objective function and techniques from structural optimization (Haftka & Gurdal, 2012) to obtain a design which is not only is capable of bearing transverse loads but also providing the desired end-point motion. Additionally, we attempt to design the flexible structure to give a desired time response by obtaining appropriate damping at the joints. The designs are obtained using a gradient-based optimization techniques.

The paper is organized as follows: In Section 2, we briefly describe the modeling of the flexible one-dimensional spine as a serial chain manipulator, and then derive the equations of motion including the effect of the springs and dampers at the joints, external loads acting on the nodes and the axial force applied at the free end. In Section 3, we analyze the optimization problem for a serial chain with two links and present the necessity of using an optimization approach for a system with large number of links. In Section 4, we frame the optimization problems for the static deflection and the dynamic response. In Section 5, we describe the numerical methods used to solve the optimization problems and present numerical results for the static and dynamic cases. We are able to show that many of the structures obtained from optimization have similar features to that of the vertebrae of fast moving quadrupeds. In Section 6, we present the conclusions, limitations and scope for further work.

2 Modeling of a multi-link flexible serial chain

Modeling and analysis of animal spine has become a focus of many research efforts related to locomotion [(Ijspeert et al., 2007), (Roos, et al., 2006)]. A realistic view of the vertebrae column would require each segment to have all six degrees-of-freedom (DoF) at each joint if the constraints due to the muscles and tendons are ignored (Christophy et al., 2013). However, this is computationally intensive. Furthermore, many of the DoFs in the 6-DoF model are unnecessary. To simplify our modeling, we consider the spine to be a multi-body serial manipulator with rigid segments and joints with some limits to the angle of rotations at the joints. We also assume that

the joints have torsional springs that offer resistance to the rotations at the joints. Figure 1 shows a N link serial chain with one end fixed and the free end subjected to a horizontal force resulting in a desired end motion. The rotations at the joints, θ_i , are with respect to a horizontal X axis and hence are absolute rotations. Each joint has an associated lumped stiffness K_i and a lumped damping C_i . At each joint, there is a loading along the negative Y axis denoted by P_Y which the structure must be capable of bearing in addition to the self-weight. The desired end motion is denoted by δ_X and this is due to a horizontal actuating force P_X that can be arbitrary.

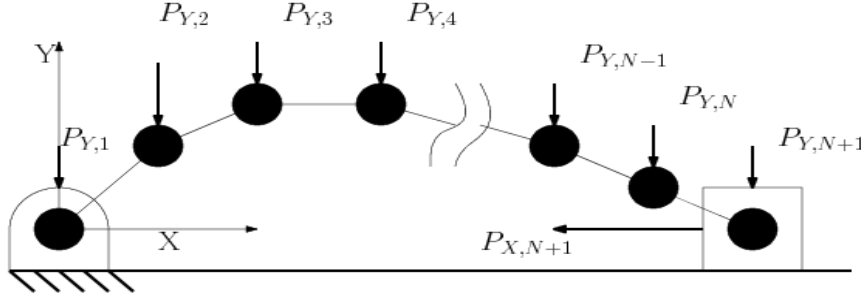


Figure 1: An N link constrained serial chain with axial and transverse loading

2.1 Equilibrium equation and equations of motion

The location of each joint (X_i, Y_i) is given by

$$X_i = \sum_{j=1}^{i-1} L_j \cos \theta_j, \quad Y_i = \sum_{j=1}^{i-1} L_j \sin \theta_j \quad (1)$$

The Y deflection of the end-point is assumed to be zero and hence there exists a constraint, denoted by $\Phi(\theta)$, of the form

$$\Phi(\theta) = \sum_{i=1}^N L_i \sin \theta_i = 0 \quad (2)$$

Denoting the deflection at the i^{th} joint along X and Y axes by ΔX_i and ΔY_i , respectively and rotation by $\delta \theta_i$, we can obtain the total potential energy as

$$PE = \frac{1}{2} \sum_{i=1}^N K_i \delta \theta_i^2 - \sum_{i=1}^{N+1} P_{X,i} \Delta X_i - \sum_{i=1}^{N+1} P_{Y,i} \Delta Y_i - \sum_{k=1}^N m_k g Y_{gk} \quad (3)$$

where, $\delta \theta_i = (\theta_i - \theta_{0,i}) - (\theta_{i-1} - \theta_{i-1,0})$, $\theta_{0,i}$ is the original orientation of the i^{th} angle, θ_i is the deformed orientation of the i^{th} angle, K_i is the torsional stiffness of the i^{th} joint, L_i is the length of the i^{th} link, $P_{X,i}$, $P_{Y,i}$ are the loads applied along X and Y axis on the i^{th} joint respectively, g is acceleration due to gravity and Y_{gk} is the position of the center of mass of the k^{th} link with mass m_k .

Associating a Lagrange multiplier λ with the constraint in equation (2), we can write the Lagrangian

$$\mathcal{L} = -PE + \lambda \Phi(\theta) \quad (4)$$

and we can generate $N + 1$ equilibrium equations by taking partial derivative with respect to states θ_i and co-state λ . We get,

$$K_m \delta \theta = \mathcal{P}(\theta) \quad (5)$$

where, $\mathcal{P}(\theta)$ denotes the load vector generated due to loadings and constraints.

For a dynamic system we use the Lagrangian ($KE - PE$) and Lagrange multiplier (Λ) with the constraint equation, to develop the equations of motion. Following the standard approach (Ghosal, 2006), the equations of motion can be written as

$$M_A(\theta)\ddot{\alpha} + C_A(\theta, \dot{\theta})\dot{\alpha} + K_A\delta\alpha = \mathcal{P}(\theta, t) \quad (6)$$

where, α is $[\theta, \Lambda]^T$ with Λ denoting the Lagrange multiplier, $M_A(\theta)$ is the augmented mass matrix, C_A is the matrix of Coriolis and damping terms, \mathcal{P} is the moment vector due to loadings and constraints. The above equilibrium equations and the equation of motion determine final states when a loading is applied. These equations will be considered as constraints for the optimization problems discussed in Section 4.

3 Analysis of the multi-link system

As mentioned earlier, the aim of this work is to design a flexible structure to withstand transverse loads and have a desired motion due to an axial load. To get an insight into the problem, we begin with a simple two-segment system as shown in Figure 2. For deriving the mathematical expression we consider the following conventions: $\theta_{0,i}$ is the unloaded orientation of the i^{th} link, $\theta_{1,i}$ is the orientation of the i^{th} link when only the vertical loading is applied, $\theta_{2,i}$ denotes the orientation of the i^{th} link when both vertical and horizontal loading is applied.

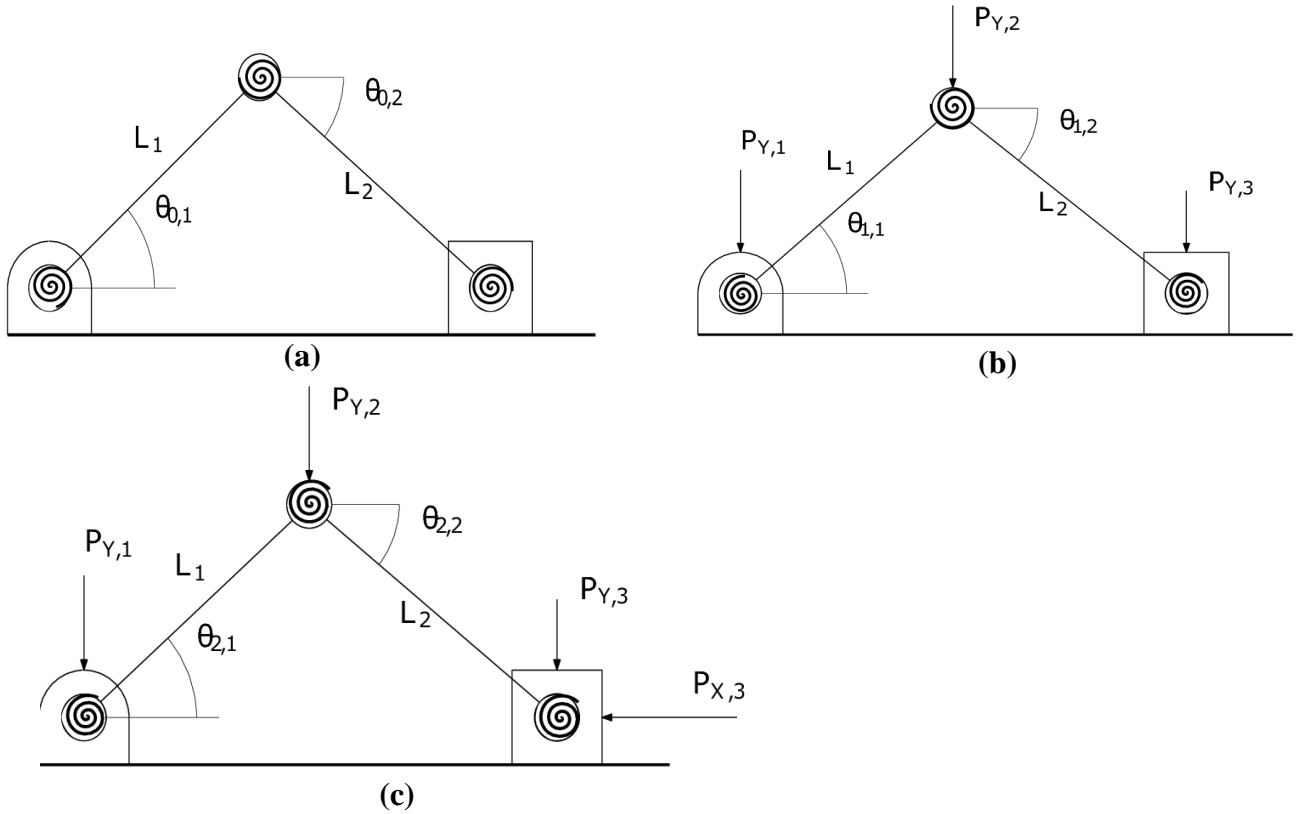


Figure 2: 2 link system with flexible node – fig (a): The unloaded structure expressed in general form, fig (b):2 link_Pa: Structure loaded by the passive loading, P_Y , fig (b):2 link_Ac: Loaded structure with the horizontal force P_X

Additionally, we remove the two springs at joint 1 and 3 and consider the two link system with only one torsional spring at the second joint with a spring stiffness denoted by K . The second joint is also loaded with a vertical force P_Y . It is prescribed that the system deflect by δ along X -axis under the action of an actuating force P_X . The link lengths are assumed to be equal and hence, $\theta_{j,1} = -\theta_{j,2} = \theta_j$. We wish to determine the undeformed angle θ_0 such that for the given

nodal stiffness, K , the end-point deflection due to the loading P_X is δ .

The static equilibrium equation for the loading conditions is given by

$$4K(\theta_1 - \theta_0) = P_Y L \cos \theta_1 \quad (7)$$

$$4K(\theta_2 - \theta_0) = -2P_X L \sin \theta_2 + P_Y L \cos \theta_2. \quad (8)$$

The end-point deflection by δ can be expressed as $L(\cos \theta_{2,1} - \cos \theta_{0,1}) + L(\cos \theta_{2,2} - \cos \theta_{0,2})$ and since $\theta_{2,1} = -\theta_{2,2} = \theta_2$, we get

$$\cos \theta_2 = \cos \theta_0 + \frac{\delta}{2L}. \quad (9)$$

For a given small δ , equations (8) and (9) can be solved in closed-form to give θ_0 in terms of K as

$$\theta_0 = \frac{1}{2} \left[\sin^{-1} \left(\frac{2P_X - \frac{4K\delta}{L^2}}{\sqrt{P_Y^2 + 4P_X^2}} \right) - \tan^{-1} \left(\frac{2P_X}{P_Y} \right) \right] \quad (10)$$

Likewise we can obtain an expression for K in terms of θ_0 as

$$K = \frac{L}{2\delta} \left(2P_X L \sin^2 \theta_0 - P_Y L \sin \theta_0 \cos \theta_0 - \frac{\delta}{2L} [2P_X L \cos \theta_0 + P_Y L \sin \theta_0] \right) \quad (11)$$

For large δ , closed-form expressions are not available and equations (8) and (9) need to be solved simultaneously using numerical techniques.

The two equations (8) and (9) are in terms of three variables θ_0 , K and δ and there exists infinitely many solutions for these three variables for a given loading P_X and P_Y . This feature makes the problem amenable to optimization of an objective function and we use the minimization of the strain energy stored in the system to obtain a unique solution. We assume that the energy stored in the system is minimum under zero axial loading, i.e., when $P_X=0$. We pose the optimization problem as follows.

$$\min_{\theta_0, K} \quad \mathcal{J} = 2K(\theta_1 - \theta_0)^2 \quad (12)$$

$$\text{Subject to} \quad \cos \theta_2 = \cos \theta_0 + \frac{\delta}{2L}$$

where θ_1 is the deflected angle obtained from equation (8) under P_Y loading, θ_2 is the deflected angle obtained from equation (8) under loading P_X and θ_0 is the undeformed angle.

From the objective function $\mathcal{J} = 2K(\theta_1 - \theta_0)^2$, we can obtain

$$\frac{\partial \mathcal{J}}{\partial K} = 2(\theta_1 - \theta_0)^2 + 4K(\theta_1 - \theta_0) \frac{\partial \theta_1}{\partial K} \quad (13)$$

$$\frac{\partial \mathcal{J}}{\partial \theta_0} = 4K(\theta_1 - \theta_0) \left(\frac{\partial \theta_1}{\partial \theta_0} - 1 \right) \quad (14)$$

From equation (7), we get

$$\frac{\partial \theta_1}{\partial K} = -\frac{4(\theta_1 - \theta_0)}{4K + P_Y L \sin \theta_1}, \quad \frac{\partial \theta_1}{\partial \theta_0} = \frac{4K}{4K + P_Y L \sin \theta_1} \quad (15)$$

and substituting the above in equation (13) we get

$$\frac{\partial \mathcal{J}}{\partial K} = 2(\theta_1 - \theta_0)^2 \left(1 - \frac{2P_Y L \sin \theta_1}{4K + P_Y L \sin \theta_1} \right)$$

$$\frac{\partial \mathcal{J}}{\partial \theta_0} = 4K(\theta_1 - \theta_0) \left(\frac{-P_Y L \sin \theta_1}{4K + P_Y L \sin \theta_1} \right) \quad (16)$$

and finally we can find the ratio of the percentage change in \mathcal{J} with respect to K and θ_0 as

$$R = \frac{2K}{\cot\theta_1 + 2(\theta_1 - \theta_0)} \quad (17)$$

Since $K \gg 1$ and as long as θ_1 is not close to zero, R is greater than 1. From this we can conclude that the objective function is more sensitive to change in θ_0 in comparison to change in K and change in shape is preferred to change in stiffness. The negative sign implies that increase in K decreases θ_1 . The preference of shape over stiffness was also seen in the numerical simulations when there are large numbers of rigid segments. We also use this observation to define a scaling C_K for the general multi-link case discussed later.

The constrained Lagrangian can be written as

$$\mathcal{L} = \mathcal{J} + \lambda_1 \left(\cos\theta_2 - \cos\theta_0 - \frac{\delta}{2L} \right). \quad (18)$$

where λ_1 is the Lagrange multiplier. The gradients with respect to the design variables can be written as

$$\frac{\partial \mathcal{L}}{\partial K} = 2(\theta_1 - \theta_0)^2 + 4K(\theta_1 - \theta_0) \frac{\partial \theta_1}{\partial K} - \Lambda_1 \sin\theta_2 \frac{\partial \theta_2}{\partial K} \quad (19)$$

$$\frac{\partial \mathcal{L}}{\partial \theta_0} = 4K(\theta_1 - \theta_0) \left(\frac{\partial \theta_1}{\partial \theta_0} - 1 \right) + \Lambda_1 \left(-\sin\theta_2 \frac{\partial \theta_2}{\partial \theta_0} + \sin\theta_0 \right) \quad (20)$$

where the derivatives are obtained from equation (8) under different loading conditions.

As $(\theta_1 - \theta_0)$ is very small hence $(\theta_1 - \theta_0)^2$ is less than $(\theta_1 - \theta_0)$. Also, $1 \leq K$, making $4K(\theta_1 - \theta_0) \geq 2(\theta_1 - \theta_0)^2$. From this it can be said that $\frac{\partial \mathcal{L}}{\partial K}$ is less than $\frac{\partial \mathcal{L}}{\partial \theta_0}$. This means that changing shape is preferred by the system to changing nodal stiffness. This behavior was also observed in many simulations, specially with larger number of links.

General form for multi-link system

The general form of the energy stored in the N link system due to the loading $P_{y,i}$, denoted by \mathcal{J} , can be written as

$$\mathcal{J} = \frac{1}{2} \Delta\theta_1^T K_m \Delta\theta_1 \quad (21)$$

where, K_m denotes the stiffness matrix and $\Delta\theta_1$ denotes the change in angle θ_0 under vertical loading only – the general form for change in angle is $\Delta\theta_k = \theta_k - \theta_0$. where, $\theta_k = [\theta_{k,1} \dots \theta_{k,i} \dots \theta_{k,N}]^T$. The constraints for general formulation are given by

$$\Phi_1 = \sum_{i=1}^N L_i \sin\theta_{0,i}$$

$$\Phi_2 = \sum_{i=1}^N L_i (\cos\theta_{2,i} - \cos\theta_{0,i}) - \delta$$

where N denotes the number of links. For the N link system, the Lagrangian, \mathcal{L} , can be written as

$$\mathcal{L} = \mathcal{J} + \lambda_1 \Phi_1 + \lambda_2 \Phi_2, \quad (22)$$

The gradient with respect to K_i is given as

$$\frac{\partial \mathcal{L}}{\partial K_i} = \frac{1}{2} \Delta\theta_1^T \frac{\partial K_m}{\partial K_i} \Delta\theta_1 + \Delta\theta_1^T K_m \frac{\partial \theta_1}{\partial K_i} - \lambda_2 \sum_{j=1}^N L_j \sin\theta_{2,j} \frac{\partial \theta_{2,j}}{\partial K_i} \quad (23)$$

and the gradient with respect to $\theta_{0,i}$ is

$$\frac{\partial \mathcal{L}}{\partial \theta_{0,i}} = \Delta \theta_1^T K_m \left[\frac{\partial \theta_1}{\partial \theta_{0,i}} - \frac{\partial \theta_0}{\partial \theta_{0,i}} \right] + \lambda_1 L_i \cos \theta_{0,i} - \lambda_2 \sum_{j=1}^N L_j \sin \theta_{2,j} \frac{\partial \theta_{2,j}}{\partial \theta_{0,i}} + \lambda_2 L_i \sin \theta_{0,i} \quad (24)$$

The expressions of $\frac{\partial \theta_k}{\partial \theta_{0,i}}, \frac{\partial \theta_k}{\partial K_i}, k = 0,1,2$ are given in Appendix I.

For the two link system without K_3 , for a small deflection, we get from equations (22)

$$K_m = \begin{bmatrix} K_1 + K_2 & -K_2 \\ -K_2 & K_2 \end{bmatrix} \quad (25)$$

$$\Delta \theta_k = \begin{bmatrix} K_1 + K_2 & -K_2 & L_1 \cos \theta_{0,1} \\ -K_2 & K_2 & L_2 \cos \theta_{0,2} \\ L_1 \cos \theta_{0,1} & L_2 \cos \theta_{0,2} & 0 \end{bmatrix}^{-1} \begin{bmatrix} P_{Y,2} L_1 \cos \theta_{0,1} - P_{X,3} L_1 \sin \theta_{0,1} \\ P_{X,3} L_2 \sin \theta_{0,2} \\ -L_1 \sin \theta_{0,1} - L_2 \sin \theta_{0,2} \end{bmatrix} \quad (26)$$

where, $k=1$ if $P_{X,3}=0$, $k=0$ if $P_{X,3}=0$ & $P_{Y,2}=0$ and $k=2$ if $P_{X,3}$ & $P_{Y,2}$ are non-zero. For small deflection,

$$\sin \theta_{j,i} = \sin \theta_{0,i} + \cos \theta_{0,i} \Delta \theta_{j,i}; \cos \theta_{j,i} = \cos \theta_{0,i} - \sin \theta_{0,i} \Delta \theta_{j,i}$$

The gradient with respect to K is given as

$$\frac{\partial \mathcal{L}}{\partial K_1} = \frac{1}{2} \Delta \theta_{1,1}^2 + \Lambda_1 \frac{\partial \Phi_1}{\partial K_1} + \Lambda_2 \frac{\partial \Phi_2}{\partial K_1}; \quad (27)$$

$$\frac{\partial \mathcal{L}}{\partial K_2} = \frac{1}{2} (\Delta \theta_{1,1} - \Delta \theta_{1,2})^2 + \Lambda_1 \frac{\partial \Phi_1}{\partial K_2} + \Lambda_2 \frac{\partial \Phi_2}{\partial K_2}; \quad (28)$$

and the gradient with respect to $\theta_{0,i}$ is given as

$$\frac{\partial \mathcal{L}}{\partial \theta_{10}} = \Delta \theta^T K_m \frac{\partial \theta_1}{\partial \theta_{10}} - \Delta \theta_1^T K_m \begin{bmatrix} 1 \\ 0 \end{bmatrix} + \Lambda_1 \frac{\partial \Phi_1}{\partial \theta_{0,1}} + \Lambda_2 \frac{\partial \Phi_2}{\partial \theta_{0,1}}; \quad (29)$$

$$\frac{\partial \mathcal{L}}{\partial \theta_{20}} = \Delta \theta_1^T K_m \frac{\partial \theta_1}{\partial \theta_{20}} - \Delta \theta_1^T K_m \begin{bmatrix} 0 \\ 1 \end{bmatrix} + \Lambda_1 \frac{\partial \Phi_1}{\partial \theta_{0,2}} + \Lambda_2 \frac{\partial \Phi_2}{\partial \theta_{0,2}}; \quad (30)$$

where,

$$\begin{aligned} \frac{\partial \Phi_2}{\partial \theta_{2,1}} &= -L_1 \sin \theta_{2,1}; & \frac{\partial \Phi_1}{\partial \theta_{0,1}} &= L_1 \cos \theta_{0,1}; \\ \frac{\partial \Phi_2}{\partial \theta_{2,2}} &= -L_2 \sin \theta_{2,2}; & \frac{\partial \Phi_1}{\partial \theta_{0,2}} &= L_2 \cos \theta_{0,2}; \\ \frac{\partial \Phi_2}{\partial \lambda} &= 0; & \frac{\partial \Phi_1}{\partial \lambda} &= 0; \end{aligned}$$

To be an optimal solution the equations (27) to (30) must be equal zero. To normalize the effects of change in stiffness and the shape, we introduce a modified stiffness K_{di} . The relationship between K_{di} and K_i is given by

$$\frac{\partial \mathcal{L}}{\partial K_{d1}} = C_K \frac{\partial \mathcal{L}}{\partial K_1}, \frac{\partial \mathcal{L}}{\partial K_{d2}} = C_K \frac{\partial \mathcal{L}}{\partial K_2}$$

where, C_K equal to 1 implies there is almost no participation of stiffness in the optimization scheme (for a large number of links) and a large C_K such as 1000 indicate that there is a significant effect of stiffness. The C_K scales the gradients to a comparable values. This allows the two type of variables to change simultaneously.

4 Optimization problems

For a multi-link system, there are no closed-form solutions just from the equilibrium equation and constraint equations. To generate an unique solution, we formulate an optimization problem. We follow the structural optimization approach as shown in Haftka & Gurdal (2012) and choose an objective function. We assume that the flexible structure must first support its own weight.

To be able to withstand its own weight, the internal strain energy (PE) stored should be minimum due to passive loading, $\mathcal{P}_1(\theta)$. We can write the internal energy stored as follows:

$$PE = \sum_{i=1}^{N+1} \frac{1}{2} K_i (\theta_{1,i-1} - \theta_{0,i-1} - \theta_{1,i} + \theta_{0,i})^2 \quad (31)$$

To achieve the desired flexibility we introduce a local constraint under active loading, $\mathcal{P}_2(\theta)$, as

$$\sum_{i=1}^N L_i (\cos(\theta_{2,i}) - \cos(\theta_{0,i})) - \delta_d = 0. \quad (32)$$

The above equation describes the end-point deflection to be δ_d if the loading condition on the structure is $\mathcal{P}_2(\theta)$. However, the loading condition \mathcal{P}_2 need not be constant with time and it could be a periodic function (as in running). We address this by considering first a constant loading condition and second a periodic loading where, the force changes as a function of time. Against a constant force we solve for the shape and stiffness under statics condition and the time response under dynamic condition. For periodic forces, we solve these two simultaneously.

4.1 Optimization problem: Static deflection

The general form for an optimization problem for an arbitrary number of segments can be posed as follows:

$$\begin{aligned} \min_{\theta_0, K_i} \quad & \mathcal{J} = \frac{1}{2} \sum_{i=1}^{N+1} K_i (\Delta\theta_{1,i} - \Delta\theta_{1,i-1})^2 \\ \text{Subjected to:} \quad & K_m(\theta_1 - \theta_0) - \mathcal{P}(\theta_1) = 0 \\ & K_m(\theta_2 - \theta_0) - \mathcal{P}(\theta_2) = 0 \\ & \sum_{i=1}^N L_i \sin\theta_{j,i} = 0; j = 0,1,2 \\ & \sum_{i=1}^N L_i (\cos(\theta_{2,i}) - \cos(\theta_{0,i})) - \delta_d = 0 \\ \text{Data:} \quad & (K_{initial}, \theta_{initial}, K_{boundary}, L_x, \delta_d) \end{aligned} \quad (33)$$

In the above, K_i are spring stiffness at the joints, $\mathcal{P}(\theta_i)$ denote the loading, L_i are the link lengths, δ_d is the desired end-point deflection along the axial direction and θ_i is the vector of joint angles at i^{th} loading condition. The constraints and ranges on θ_0 and K are based on informed guess-work as there no data available for these type of problem from a biological system or a robot (see also Section 5).

In Section 3 to study the relative effect of stiffness (K) and orientation (θ_0), we had introduced a factor C_K . In terms of this factor, we can frame the optimization problem as

$$\min_{\theta_0, C_K^{-1}K_i} \mathcal{J} = \frac{1}{2} \sum_{i=1}^{N+1} K_i (\Delta\theta_i - \Delta\theta_{i-1})^2 \quad (34)$$

where, C_K is the factor that equalizes stiffness magnitude to the radians. This allows the system to change both the stiffness and orientation simultaneously. In Section 5, we use a gradient based technique to solve the aforementioned optimization problem.

4.2 Optimization problem: Dynamic response time

For the dynamic case, we assume a constant actuation at the endpoint and determine the response time of the structure. To remove oscillations within the structure we ensure the structure to be over-damped by adjusting the lower limit of the damping coefficient. To control the time response against the constant loading, we introduce the square of the damping coefficient to be the objective function.

Under large dissipative forces in the system, the end-point motion behavior is similar to the equation of $(1 - e^{-at})$. To control the rise time, we consider a cutoff value¹ from the equilibrium value – we have assumed Δ_{cutoff} as 0.9 times the deflection value at equilibrium, δ_d . The optimization problem for the dynamic case can be framed as

$$\begin{aligned} \min_{\vec{C}_v} & \quad \frac{\Lambda}{2} \vec{C}_v^T \vec{C}_v \\ \text{Subjected to} & \quad M(\theta)\ddot{\theta} + C_r(\theta, \dot{\theta})\dot{\theta} + C \dot{\theta} + K(\theta - \theta_0) - \mathcal{P}(\theta) = 0 \\ & \quad \frac{1}{2}(t_{end} - T_d)^2 = 0 \\ \text{Data:} & \quad C_{initial}, C_{boundary}, T_d \end{aligned} \quad (35)$$

In the above, C_v denotes the damping and as in the static optimization, we assume a reasonable range for damping – in our simulation we have assumed $1 \leq C_{v,i} \leq 10^3$. C_r contains the Coriolis force terms, C contains the damping terms, K contains all the stiffness terms. The optimization problem in equation (35) is solvable because there exists a direct closed-form relationship between the constraints (cut-off time and end-point deflection). The end-point deflection is given by

$$\begin{aligned} \delta x(t) &= \delta_d (1 - e^{-\tau t}) \\ \text{where } \tau &= -\frac{1}{T_d} \ln\left(\frac{\Delta_{cutoff}}{\delta_d}\right) \end{aligned} \quad (36)$$

Here, $\delta x(t)$ is the end-point deflection with time, Δ_{cutoff} is the magnitude deflection

¹ We use *eventfunction* is Matlab (MATLAB, 2012) during numerical simulations.

corresponding to time T_d . Δ_{cutoff} and T_d are two user prescribed values determine the response time of the end-point motion against a constant loading. The lower limit of the nodal damping is set, through trial and error, to ensure the end-point motion will be always a second order over damped motion. To simplify our approach we directly assume the motion to be a 1st order motion and make predictions about the response. This assumptions are backed by numerical results described in Section 5.

In a combined static and dynamic optimization case, we consider the forcing function to be periodic with a frequency of $\frac{\Omega}{2\pi}$ Hz. Our objective is to generate a set of parameters of the N link system that will satisfy our demand for a maximum deflection of δ_d while maintaining minimum strain energy under passive loading. The optimization problem can be stated as follows:

$$\begin{aligned}
& \min_K && \frac{1}{2} \sum_{i=1}^{N+1} K_i (\Delta\theta_{1,i} - \Delta\theta_{1,i-1})^2 \\
& \text{Subjected to} && K(\theta_1 - \theta_0) - \mathcal{P}(\theta_1) = 0 \\
& && \mathcal{M}(\theta_2)\ddot{\theta}_2 + \mathcal{C}(\theta_2, \dot{\theta}_2)\dot{\theta}_2 + K(\theta_2 - \theta_0) + \mathcal{C}(\theta_2) - \mathcal{P}(\theta_2, \Omega t) = 0 \quad (37) \\
& && \min(\sum_{i=1}^N L_i (\cos(\theta_{2,i}) - \cos(\theta_{0,i}))) - \delta_d = 0 \\
& \text{Data:} && (K_{initial}, \theta_{initial}, K_{boundary})
\end{aligned}$$

It can be observed that the above combined optimization problem involves a differential equation (equation of motion) as a constraint. In addition, a constraint involving a minimum is also present. A gradient-based optimization might not yield results if the constraints contain a maximum or minimum value from a series of data and a genetic algorithm or pattern search yields more effective results (Deb, 1999). We have used genetic algorithm to generate the solution for the combined dynamic problem.

5 Numerical methods and results

The optimization problems in equations (33) and (35) were solved in Matlab (MATLAB, 2012) using *fmincon* which is a gradient based optimization procedure. However the optimization problem in equation (37) could not be solved using *fmincon* and we have used genetic algorithm and pattern search. We have used Matlab (MATLAB, 2012) library function *ga* and *patternsearch* for implementing genetic algorithm and pattern search. The length of each link along X -axis are assumed to be equal and given by L_x/N m with L_x as the total length of the flexible spine and N is the number of links. Apart from the constraints described earlier, we list below additional constraints and choices made for the numerical simulations which make the solutions more reasonable.

Geometrical and stiffness values

We have used the following constraints and ranges for the geometrical and stiffness variables in all the numerical simulations.

- Length constraint: $L_i = \frac{L_{x,i}}{\cos\theta_{0,i}}$
- Angle constraint: $-\frac{\pi}{6} \leq \theta_{i0} \leq \frac{\pi}{6}$
- Relative angle constraint: $-\frac{\pi}{6} \leq \theta_{0,i} - \theta_{0,i+1} \leq \frac{\pi}{6}$
- Stiffness limit: $10^2 \leq K_i \leq 10^4$

- Geometric upper and lower limit: $0.01 \leq Y_{0,i} \leq 0.25L_x$

The upper and lower bound of the nodal stiffness is based on the study done by Lavaste and Mazel (Lavaste et al., 1992). They state the average approximate torsional stiffness against flexion to be $3 N - m/deg$ or $172 N - m/rad$ for spine motion segment. We have used 100 N-m/rad as the lower bounds and 1000 N-m/rad as the upper bound for the stiffness value at the joints. The upper limit of $Y_{0,i}$ is an user prescribed criteria as no such number is available in literature. Like wise the choice lower limit of $Y_{0,i}$ is also arbitrary. The only constraint on the lower limit is to ensure that the Y value is not negative. The initial orientation, $\theta_{0,i}$, is constrained to ensure link length dimension $L_{link} = \frac{L_{x,i}}{\cos\theta_{0,i}}$ is reasonable. If $\theta_{0,i}$ is large then the link length can be come very large and we have constrained $\theta_{0,i}$ to be between $\pm\pi/6$. The local orientation, $(\theta_{0,i} - \theta_{0,i-1})$, constraint prohibits the structure from generating sharp changes in rotation between two links or form knots when there is a large number of links.

Applied force value selection

To the best of our knowledge there are no estimates for the applied axial force in a moving quadruped robot and likewise in the muscles of a fast moving animal. It is known in literature (Sanchis-Moysi et al., 2010) that for an active young adult male tennis player, the volume of the muscle is approximately 480 cm^3 and in a study done by Akagi and Fukunaga (Akagi, et al., 2009), it is mentioned that a 350 cm^3 muscle generates approximately 76 N-m of torque. Dividing this number with the arm length, the force generated by the muscle, at it's peak, is about 310 N of force. In our simulations, we have assumed the axial force, $P_{x,2}(N + 1,1)$ as - 400 N. However, any other value could also be used.

5.1 Static optimization

The solutions to the optimization for different static loading and different number of rigid segments is presented here. As stated in Section 4, the initial angles and the nodal stiffness are considered as the design variables. We solve for the optimal values for 5 and 10 rigid segments. The simulation is conducted under an uniform vertical loading of -10 N/node for 5 segment system and -5 N/node for the 10 segment system. The horizontal force applied at the end node is -400 N. The initial solution provided for the optimization problem, for 5 link system, is $\{\frac{\pi}{5}, 0, 0, 0, -\frac{\pi}{5}, 10000, 250, 250, 250, 250, 0\}$. The results of the static optimization problem described in equation (12) are shown in figure 3.

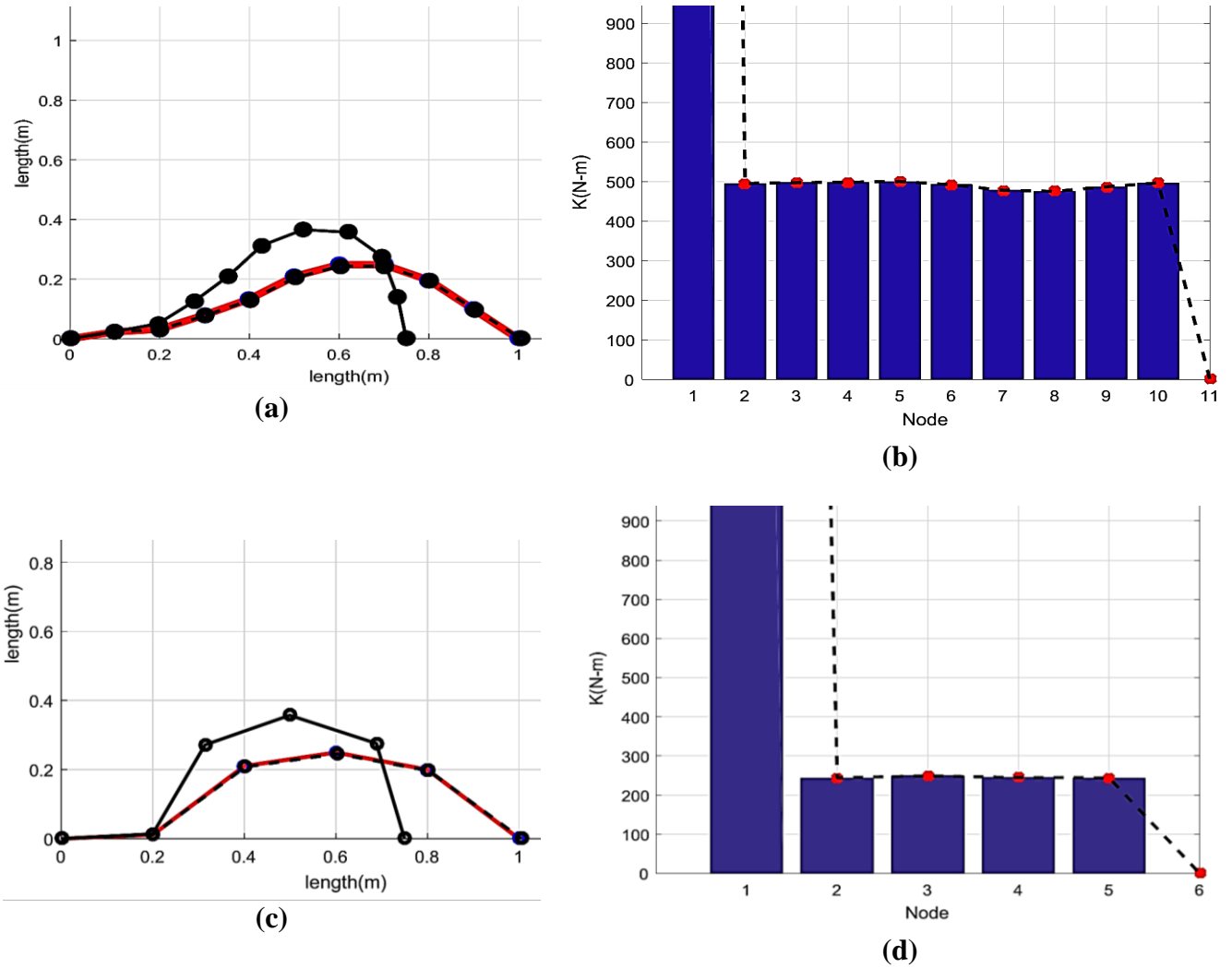
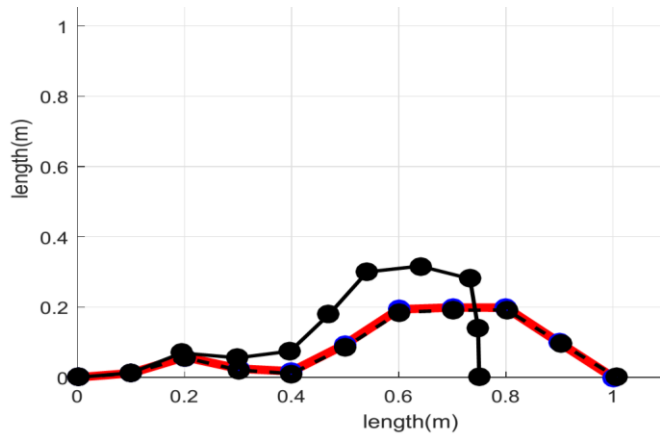
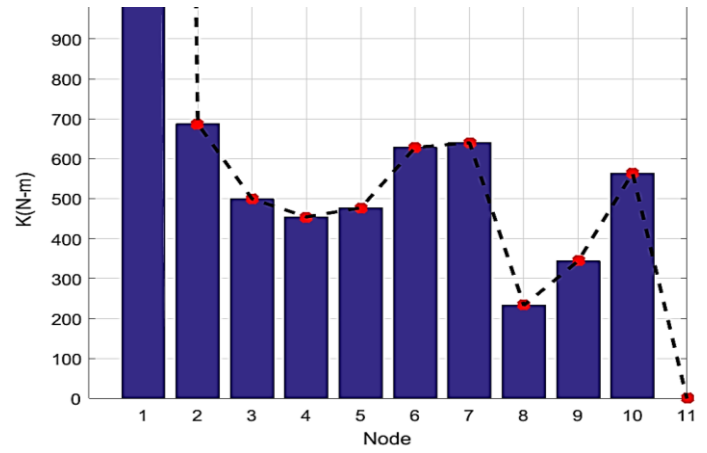


Figure 3: (a) Undeformed and deformed structure of a 10 segment system, (b) The nodal stiffness of the structure, (c) Undeformed and deformed structure of a 5 segment system, (d) The nodal stiffness of the structure.

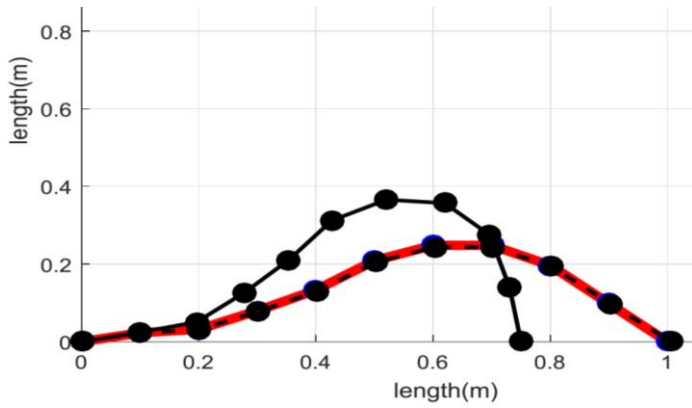
Next, we demonstrate the localized stiffening of the structure and end-point motion indifference to the variation of localized loading. The number of rigid segments chosen is 10. The vertical loading at every node from 1 to 5 is -20 N and all other nodes loading force is -5 N. While the horizontal axial loading is -400 N at the end node. The results described in Fig. 3 and Fig. 4 are for similar conditions, except in Fig. 4, the vertical loading is same at all nodes.



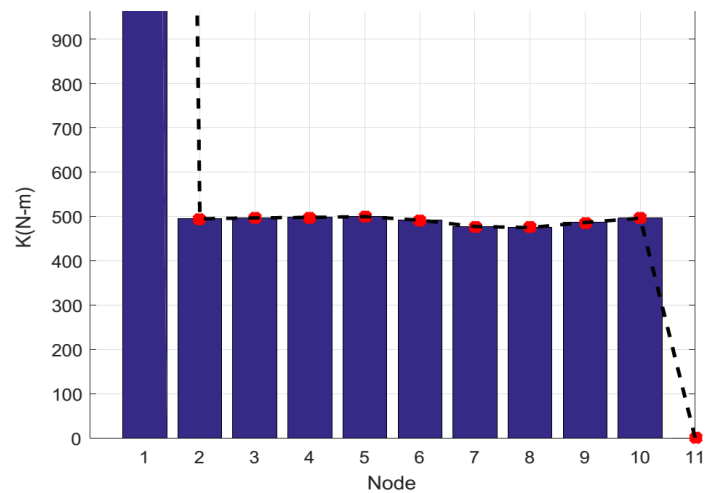
(a)



(b)



(c)



(d)

Figure 4: (a,b) Node 1 to Node 5, -20 N per node, rest -5 N per node and (c,d) Uniformly loaded with -5 N per node

From the results displayed in figure 4, it can be seen by changing the orientation of links of the loaded region the effect of the extra load is mitigated and end effector motion remains unchanged. This validates our claim of "localized stiffening of the structure and end-point motion indifference to the variation of localized loading". In Fig. 5, the shape and stiffness of the structure for various loads at the nodes are shown.

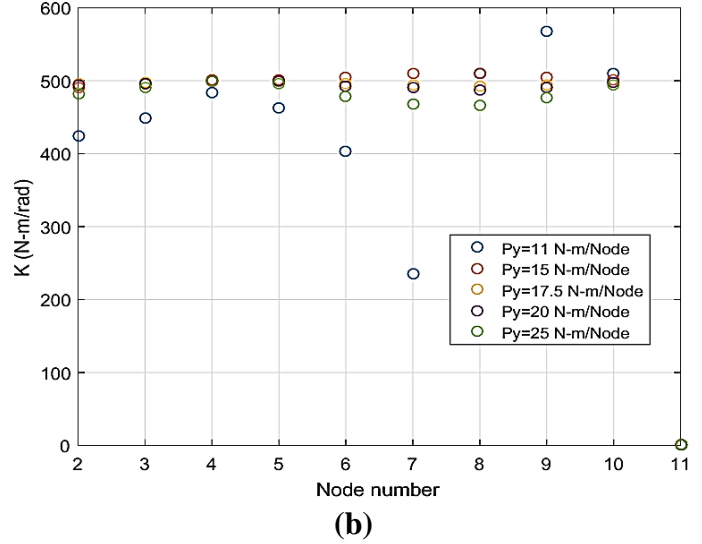
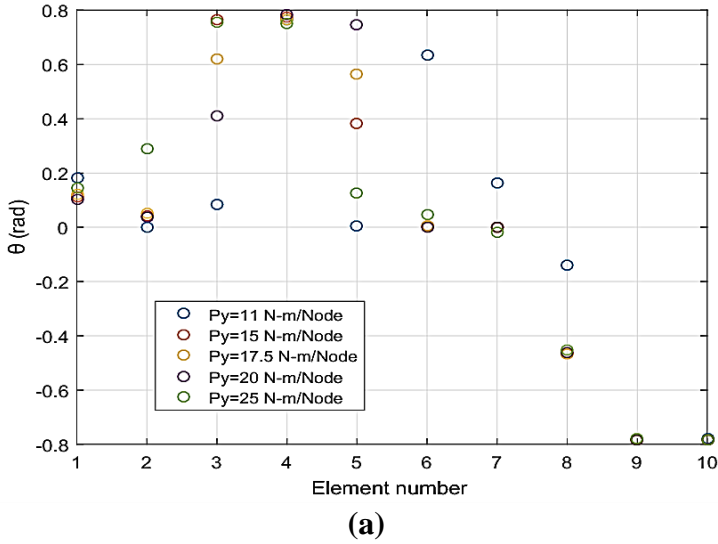


Figure 5: (a) Variation of design variable θ_0 under various loading condition and (b) Variation of design variable K under various loading condition

The factor C_K in the optimization problem changes the gradient with respect to the modified nodal stiffness. This is similar to putting a cost on the design parameters. A very high C_K means the cost of changing stiffness is high compared to the cost of changing orientation and vice versa. This idea can be verified by the variation of shape (Fig: 6 to 8) and variation of stiffness (Fig: 6 to 8). As the C_K is increased the stiffness variation between the nodes increases where as the change in orientation of the links is less apparent.

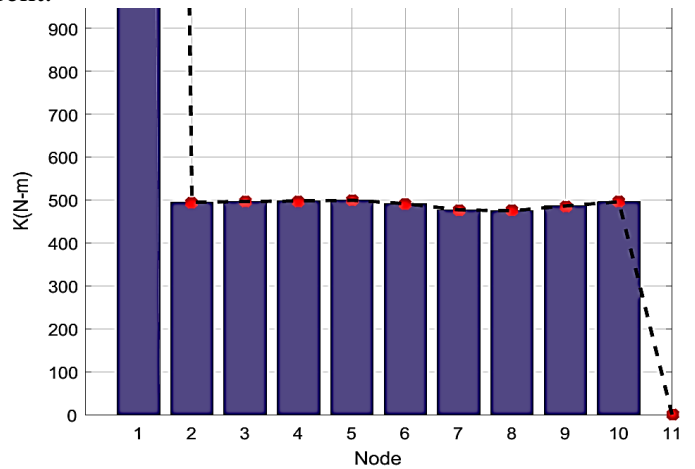
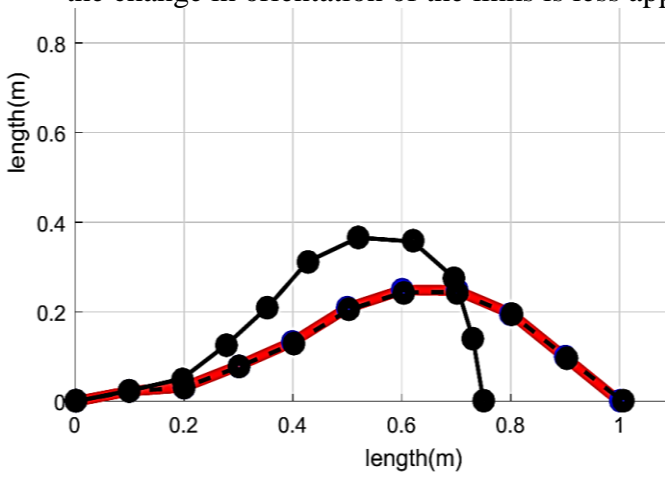


Figure 6: $C_K=1$, Transverse loading $-5N$ per node, Link no. 10, Axial loading $-400N$

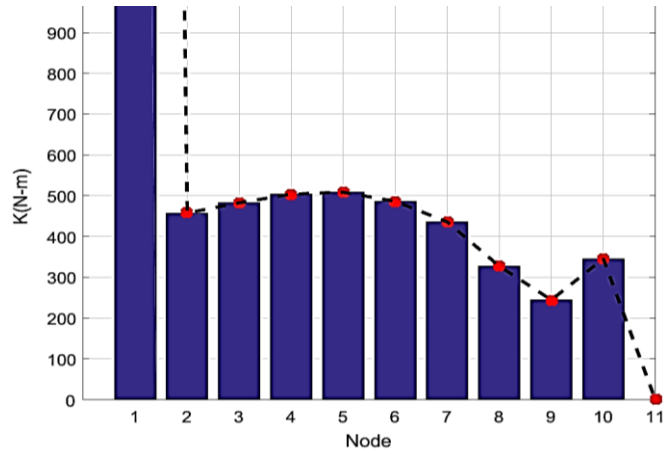
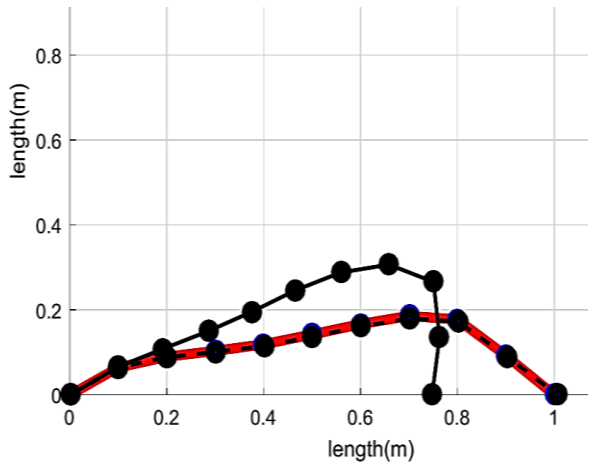


Figure 7: $C_K=10^2$, Transverse loading -5N per node, Link no. 10, Axial loading -400 N

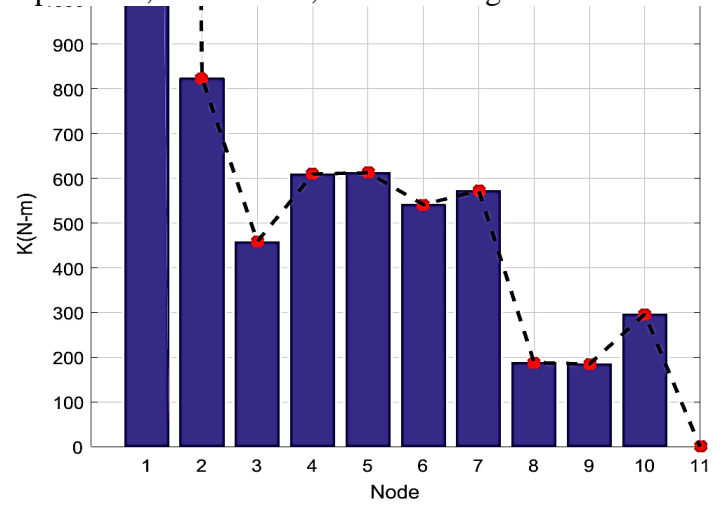
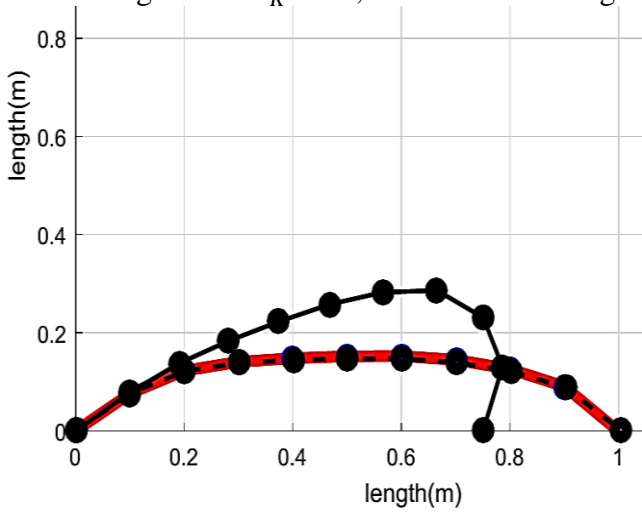


Figure 8: $C_K=10^4$, Transverse loading -5N per node, Link no. 10, Axial loading -400 N

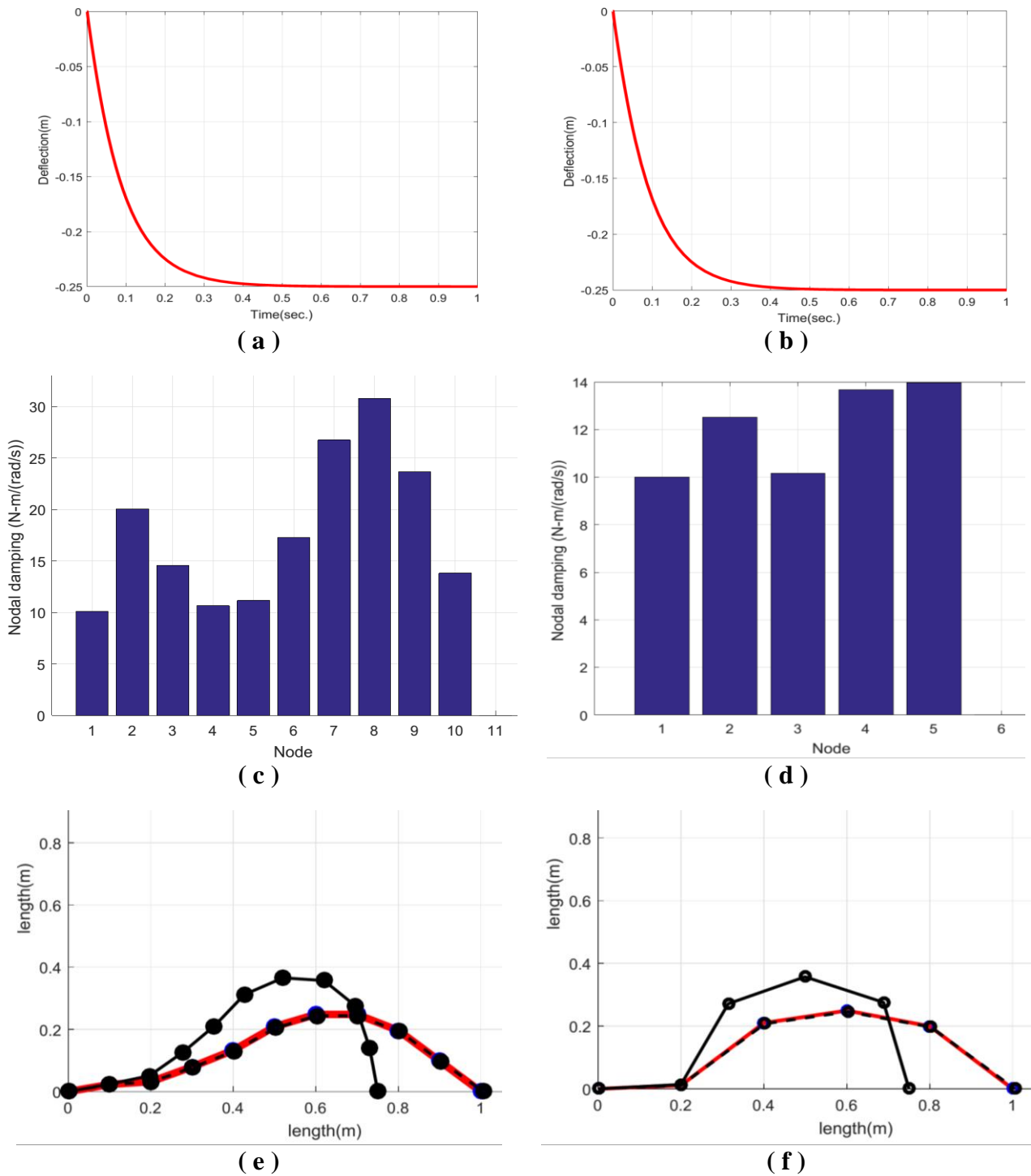


Figure 9: (a) End-point response of structure with 10 link, (c) Nodal damping of the 10 link system, (e) Undeformed and deformed structure of a 10 link system, (b) End-point response of structure with 5 link, (d) Nodal damping of the 5 link system, (f) Undeformed and deformed structure of a 5 link system

5.2 Dynamics

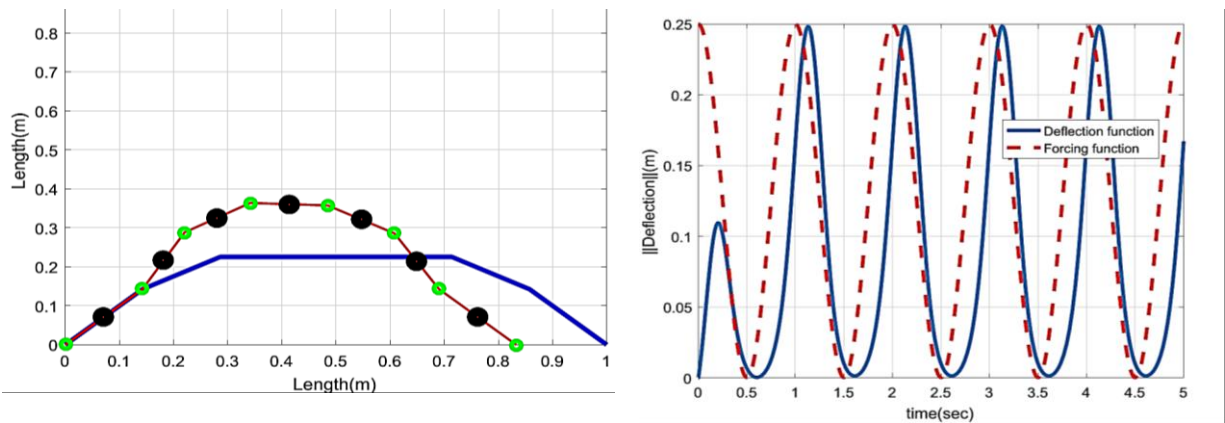
In this section we describe the results related to the response of the structure for constant and periodic loading. We consider the structures obtained from the static optimization process under the prescribed static loading condition and attempt to control their response time by parameter optimization. Towards the end of this section we show that a structure obtained from static optimization process can also be used with periodic loading if the response time of the structure is fast enough.

5.2.1 Case 1: Application of constant force

In real world scenario the structure deforms over a certain amount of time before it attains equilibrium for a constant force. By adjusting the nodal damping we can predict the response of the structure. The results, figure 9, describe the response of a 5-link and a 10-link structure, fixed at one end and free at the other, when actuated by a constant force. As it can be seen from equation (36) one can predict the response of the structure quite accurately. The time constant of the structure is obtained as $\tau = 11.5 \text{ sec}^{-1}$.

5.2.2 Case 2: Application of periodic force

We optimize the structure for a periodic end force to simulate rapid and periodic movement of the end-point. The number of links chosen for this simulation is 7 and we use a genetic algorithm for optimization in this case. The vertical loading on each node is assumed to be -50 N and from node 2 to 4 it is assumed as -100 N. The horizontal loading is chosen to be -4000 N. We assume the nodal damping as 50 N-m/(rad/s) and mass of the links as 0.5 kg. The results from optimization are shown in figure 10. It can be seen that the end-point reaches the desired δ in 0.5 seconds. However, when the load is removed the structure returns to its original state in about 0.25 seconds. This result indicates that the release of stored energy is much faster.



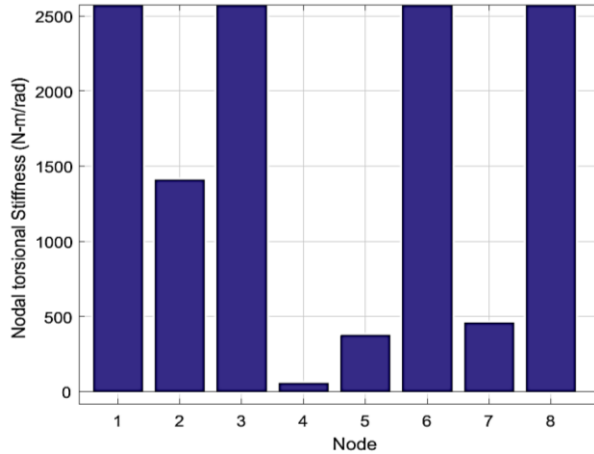
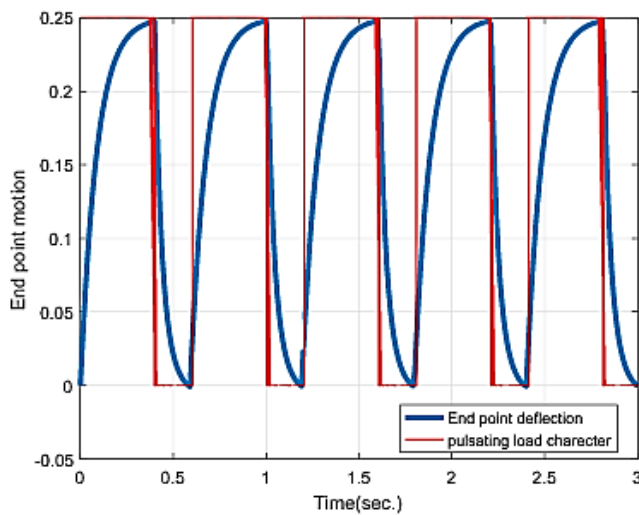


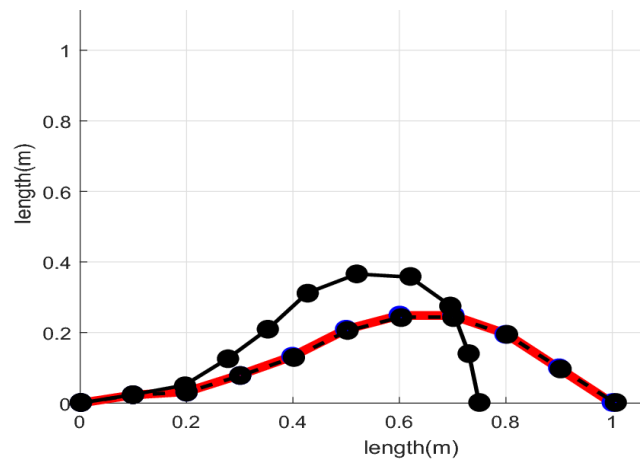
Figure 10: 7 link structure Nodal stiffness optimization under dynamic loading

5.2.2 Fast responsive constant load solution

Figure 11 shows the response of the 10-link structure obtained using gradient-based optimization algorithms. Comparing this result with that obtained by genetic algorithm shows that for a fast responsive structure, the response at the end-point is similar. The gradient-based approach is however much faster for simulation.

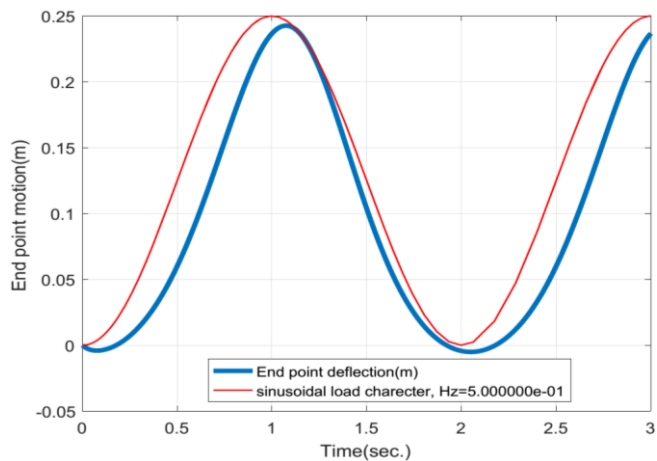


(a)

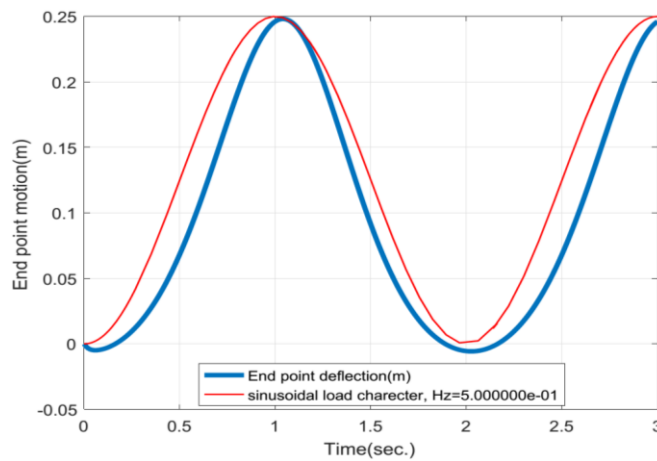


(b)

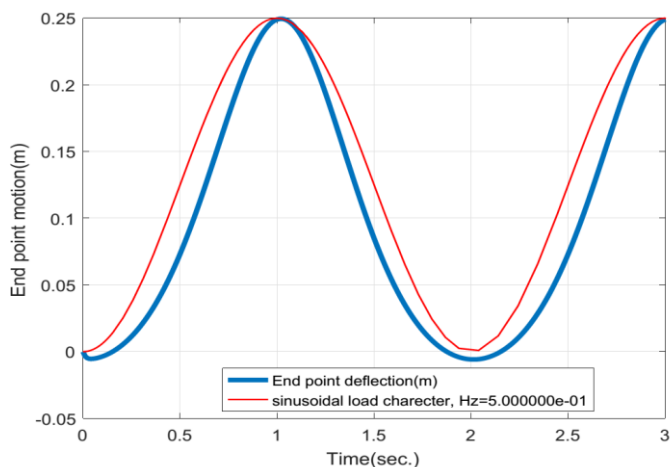
Figure 11: (a) Pulsating oscillation and its corresponding end-point motion, (b) Structure responding to the oscillation.



(a)



(b)



(c)

Figure 12: (a) Response time 0.2s for 90% of the maximum deflection, (b) Response time 0.1s for 90% of the maximum deflection, (c) Response time 0.05s for 90% of the maximum deflection.

As can be seen, from Fig. 11 and Fig 12., fast responsive structure can generate motion as per our requirement even if the actuating force is not constant. This approach is valid only for loading patterns with lower frequency. With a small modification in the actuating force application we can achieve structure supporting fast locomotion with static optimization.

It has been observed from extensive simulations that the general optimization problem, equation (33), is non-convex . Thus, there are many solutions. Secondly, in all the numerical simulations we have used a chosen set of parameter values based on informed guess-work and literature. The gradient based or the genetic algorithm based solution procedure is in no way limited by these choices and can be used for other parameter values.

6 Conclusions

This paper deals with modeling and numerical simulation of flexible one-dimensional structures subjected to transverse loading and with a prescribed axial displacement. This work is motivated by the need to model and analyze flexible spines in animals and in quadruped robots as this gives increased speed and agility. The flexible structure is modeled as a series of rigid segments with

springs and dampers at the joints. For such a system of rigid segments subjected to transverse and axial loading, the structure can take up an infinite number of configurations and the joint variables are not unique. We solve the problem by posing it as an optimization problem. For the static loading, we minimize an objective function related to the strain energy of the system. For the constant dynamic loading, we minimize an objective function involving the damping at the joints, which in turn determines the response time of the system. The first two optimization problem are solved using a gradient based approach. The periodic case is solved using genetic algorithm and pattern search. Numerical results are obtained to illustrate the optimization problems. The main results are a) the change in orientation is preferred to change in stiffness at the joints and b) the change is more pronounced near the point of end-point load. For the simulations, we have used numerical values and ranges on the data based on informed guess-work as data on animals and robots are not readily available. The formulations and approach developed in this paper can be, however, applied for any data sets. This work deals with planar structures and for future work, we intend to extend the approach to model and analyze 3D motion of structures.

Appendix I: Gradients

In this Appendix, the details of the mathematics for the case of large deflection case are presented.

The internal energy stored due to the passive loading is \mathcal{J} . This and the constraints, Φ_1 Φ_2 are given as

$$\mathcal{J} = \frac{1}{2} \Delta\theta_1^T K_m \Delta\theta_1. \quad (38)$$

$$\Phi_1 = \sum_{i=1}^N L_i \sin\theta_{0,i} \quad (39)$$

$$\Phi_2 = \sum_{i=1}^N L_i (\cos\theta_{2,i} - \cos\theta_{0,i}) \quad (40)$$

where, θ_0 is the vector of initial undeformed angles, $\Delta\theta_1$ is the vectors of the angular deflection due to the passive loading $\mathcal{P}(\theta_1)$, θ_2 is the vectors of the final state of the angles due to the passive and active loading combined, $\mathcal{P}(\theta_2)$. Combining all the constraints and objective function we generate the Lagrangian. It is given by

$$\mathcal{L} = \mathcal{J} + \Lambda_1 \Phi_1 + \Lambda_2 \Phi_2 \quad (41)$$

where, Λ_1, Λ_2 are Lagrange multipliers. Now we compute the gradients of the Lagrangian with respect to the design variables (K, θ_0) . Here K is a $(N + 1 \times 1)$ vector, and θ_0 in a $(N \times 1)$ vector. $K_i, \theta_{0,i}$ are the i^{th} element of the vectors. The gradient with respect to individual elements are as followed.

$$\frac{\partial \mathcal{L}}{\partial K_i} = \frac{\partial \mathcal{J}}{\partial K_i} + \Lambda_1 \frac{\partial \Phi_1}{\partial K_i} + \Lambda_2 \frac{\partial \Phi_2}{\partial K_i} \quad (42)$$

$$= \frac{\partial \mathcal{J}}{\partial K_i} - \Lambda_2 \sum_{j=1}^N L_j \sin\theta_{2,j} \frac{\partial \theta_{2,j}}{\partial K_i} \quad (43)$$

$$= \frac{1}{2} \Delta\theta_1^T \frac{\partial K_m}{\partial K_i} \Delta\theta_1 + \Delta\theta_1^T K_m \frac{\partial \theta_1}{\partial K_i} - \Lambda_2 \sum_{j=1}^N L_j \sin\theta_{2,j} \frac{\partial \theta_{2,j}}{\partial K_i}$$

$$\begin{aligned} \frac{\partial \mathcal{L}}{\partial \theta_{0,i}} &= \frac{\partial \mathcal{J}}{\partial \theta_{0,i}} + \Lambda_1 \frac{\partial \Phi_1}{\partial \theta_{0,i}} + \Lambda_2 \frac{\partial \Phi_2}{\partial \theta_{0,i}} \\ &= \frac{\partial \mathcal{J}}{\partial \theta_{0,i}} + \Lambda_1 L_i \cos\theta_{0,i} - \Lambda_2 \sum_{j=1}^N L_j \sin\theta_{2,j} \frac{\partial \theta_{2,j}}{\partial \theta_{0,i}} + \Lambda_2 L_i \sin\theta_{0,i} \end{aligned} \quad (44)$$

$$= \Delta\theta_1^T K_m \left[\frac{\partial \theta_1}{\partial \theta_{0,i}} - \frac{\partial \theta_0}{\partial \theta_{0,i}} \right] + \Lambda_1 L_i \cos\theta_{0,i} - \Lambda_2 \sum_{j=1}^N L_j \sin\theta_{2,j} \frac{\partial \theta_{2,j}}{\partial \theta_{0,i}} + \Lambda_2 L_i \sin\theta_{0,i} \quad (45)$$

$$\begin{pmatrix} \frac{\partial \theta_2}{\partial K_i} \\ \frac{\partial \lambda}{\partial K_i} \end{pmatrix} = \begin{bmatrix} K_m - \nabla_{\theta_2} \mathcal{P}(\theta_2) & -\frac{\partial \mathcal{P}(\theta_2)}{\partial \lambda} \\ \nabla_{\theta_2} \Phi_3^T & 0 \end{bmatrix}^{-1} \begin{pmatrix} -\frac{\partial K_m}{\partial K_i} \Delta \theta_2 \\ 0 \end{pmatrix} \quad (46)$$

$$\begin{pmatrix} \frac{\partial \theta_2}{\partial \theta_{0,i}} \\ \frac{\partial \lambda}{\partial \theta_{0,i}} \end{pmatrix} = \begin{bmatrix} K_m - \frac{\partial \mathcal{P}(\theta_2)}{\partial \theta_2} & -\frac{\partial \mathcal{P}(\theta_2)}{\partial \lambda} \\ \nabla_{\theta_2} \Phi_3^T & 0 \end{bmatrix}^{-1} \begin{pmatrix} K_m \frac{\partial \theta_0}{\partial \theta_{0,i}} \\ 0 \end{pmatrix}.$$

where, K_m is the stiffness matrix used in equilibrium equation. The form of K_m is given as follows:

$$K_m = \begin{bmatrix} K_1 + K_2 & -K_2 & \cdot & \cdot & 0 & 0 \\ -K_2 & K_2 + K_3 & -K_3 & \cdot & \cdot & 0 \\ \cdot & \cdot & \cdot & \cdot & \cdot & \cdot \\ \cdot & \cdot & -K_i & K_i + K_{i+1} & -K_{i+1} & \cdot \\ \cdot & \cdot & \cdot & \cdot & \cdot & \cdot \\ 0 & \cdot & \cdot & -K_{N-1} & K_{N-1} + K_N & -K_N \\ 0 & 0 & \cdot & \cdot & -K_N & K_N + K_{N+1} \end{bmatrix} \quad (47)$$

here, λ represents the Lagrange multiplier introduced for the constraint, equation (33), to generate the equilibrium equations. The Λ_i and λ are of generated from two different optimization problems. The constraint for the large deflection, Φ_3 ,

$$\Phi_3 = \sum_{i=1}^N L_i \sin \theta_i.$$

$$\nabla_{\theta} \Phi_3 = \begin{pmatrix} \cdot \\ \cdot \\ L_j \cos \theta_j \\ \cdot \\ \cdot \end{pmatrix}$$

P_X and P_Y are vectors containing the forces applied at the nodes along X-axis and Y-axis. For the problem discussed, other than $P_{X,N+1}$ all other $P_{X,i}$ are zeros. The load vector for the equilibrium equation for large deflection is as followed.

$$\begin{aligned} \mathcal{P}(\theta) &= \mathcal{L}_c \mathcal{A} P_Y - \mathcal{L}_s \mathcal{A} P_X + \lambda \nabla_{\theta} \Phi_3; \\ \frac{\partial \mathcal{P}}{\partial \theta_i} &= \frac{\partial \mathcal{L}_c}{\partial \theta_i} \mathcal{A} P_Y - \frac{\partial \mathcal{L}_s}{\partial \theta_i} \mathcal{A} P_X + \lambda \frac{\partial \nabla_{\theta} \Phi_3}{\partial \theta_i}; \end{aligned} \quad (48)$$

$$\begin{aligned} &= \frac{\partial \mathcal{L}_c}{\partial \theta_i} \begin{bmatrix} \cdot \\ \cdot \\ \sum_{j=k}^{N+1} P_{Y,j} \\ \cdot \\ \cdot \end{bmatrix} - \frac{\partial \mathcal{L}_s}{\partial \theta_i} \begin{bmatrix} \cdot \\ \cdot \\ \sum_{j=k}^{N+1} P_{X,j} \\ \cdot \\ \cdot \end{bmatrix} - \lambda \begin{pmatrix} 0 \\ \cdot \\ L_i \sin \theta_i \\ \cdot \\ 0 \end{pmatrix}; \\ &= - \begin{bmatrix} 0 \\ \cdot \\ \sum_{j=i}^{N+1} (P_{Y,j} L_i \sin \theta_i + L_i \cos \theta_i P_{X,j}) + \lambda L_i \sin \theta_i \\ \cdot \\ \cdot \\ 0 \end{bmatrix} \end{aligned} \quad (49)$$

$$\frac{\partial \mathcal{P}}{\partial \lambda} = \nabla_{\theta} \Phi_3. \quad (50)$$

where,

$$\mathcal{L}_C = \begin{bmatrix} L_1 \cos \theta_1 & 0 & \cdot & \cdot & 0 & 0 \\ 0 & L_2 \cos \theta_2 & 0 & \cdot & \cdot & 0 \\ \cdot & 0 & L_3 \cos \theta_3 & 0 & \cdot & \cdot \\ \cdot & \cdot & 0 & L_i \cos \theta_i & 0 & \cdot \\ 0 & \cdot & \cdot & 0 & L_{N-1} \cos \theta_{N-1} & 0 \\ 0 & 0 & \cdot & \cdot & 0 & L_N \cos \theta_N \end{bmatrix} \quad (51)$$

$$\mathcal{L}_S = \begin{bmatrix} L_1 \sin \theta_1 & 0 & \cdot & \cdot & 0 & 0 \\ 0 & L_2 \sin \theta_2 & 0 & \cdot & \cdot & 0 \\ \cdot & 0 & L_3 \sin \theta_3 & 0 & \cdot & \cdot \\ \cdot & \cdot & 0 & L_i \sin \theta_i & 0 & \cdot \\ 0 & \cdot & \cdot & 0 & L_{N-1} \sin \theta_{N-1} & 0 \\ 0 & 0 & \cdot & \cdot & 0 & L_N \sin \theta_N \end{bmatrix} \quad (52)$$

$$\mathcal{A} = \begin{bmatrix} 1 & 1 & \cdot & \cdot & 1 & 1 \\ 0 & 1 & 1 & \cdot & \cdot & 1 \\ 0 & 0 & 1 & \cdot & \cdot & 1 \\ \cdot & \cdot & \cdot & \cdot & \cdot & \cdot \\ 0 & \cdot & \cdot & 0 & 1 & 1 \\ 0 & 0 & \cdot & \cdot & 0 & 1 \end{bmatrix} \quad (53)$$

Appendix II: Gradients of Equation (33):

In the equation (33) we describe the optimization problem under static loading. The Lagrangian is written as

$$\mathcal{L} = \mathcal{J} + \Lambda_1 \mathcal{C}_1 + \Lambda_2 \mathcal{C}_2 + \Lambda_3 \mathcal{C}_3 + \Lambda_4 \mathcal{C}_4$$

Where,

$$\begin{aligned} \mathcal{J} &= \frac{1}{2} \sum_{i=1}^N K_i (\Delta \theta_{1,i} - \Delta \theta_{1,i-1})^2 \\ \mathcal{C}_1 &= \mathbb{K}_m \Delta \theta_1 - \mathbb{P}(\theta_1), \mathcal{C}_2 = \mathbb{K}_m \Delta \theta_2 - \mathbb{P}(\theta_2) \\ \mathcal{C}_3 &= \begin{pmatrix} \sum_{i=1}^N L_i \sin \theta_{i,0} \\ \sum_{i=1}^N L_i \sin \theta_{1,i} \\ \sum_{i=1}^N L_i \sin \theta_{2,i} \end{pmatrix} \\ \mathcal{C}_4 &= \sum_{i=1}^N L_i (\cos \theta_2 - \cos \theta_0) - \delta \end{aligned}$$

The gradients of the Lagrangian, \mathcal{L} , determines the optimization process. When $\frac{\partial \mathcal{L}}{\partial K_i}$ and $\frac{\partial \mathcal{L}}{\partial \theta_{0,i}}$ reaches zero the optimization process provides the result

$$\frac{\partial \mathcal{L}}{\partial K_i} = \frac{\partial \mathcal{J}}{\partial K} + \sum_{j=1}^4 \Lambda_j^T \frac{\partial C_j}{\partial K_i}$$

$$\frac{\partial \mathcal{L}}{\partial \theta_{0,i}} = \frac{\partial \mathcal{J}}{\partial \theta_{0,i}} + \sum_{j=1}^4 \Lambda_j^T \frac{\partial C_j}{\partial \theta_{0,i}}$$

where,

$\frac{\partial \mathcal{J}}{\partial K_i} = \frac{\partial \mathcal{J}}{\partial K_i} + \sum_{j=1}^N \frac{\partial \mathcal{J}}{\partial \theta_{1,j}} \frac{\partial \theta_{1,j}}{\partial K_i}$	$\frac{\partial \mathcal{J}}{\partial \theta_{0,i}} = \frac{\partial \mathcal{J}}{\partial \theta_{0,i}} + \sum_{j=1}^N \frac{\partial \mathcal{J}}{\partial \theta_{1,j}} \frac{\partial \theta_{1,j}}{\partial \theta_{0,i}}$
$\frac{\partial C_1}{\partial K_i} = \frac{\partial \mathbb{K}_m}{\partial K_i} \Delta \theta_1 + \mathbb{K} \frac{\partial \Delta \theta_1}{\partial K_i} - \frac{\partial \mathbb{P}(\theta_1)}{\partial K_i}$	$\frac{\partial C_1}{\partial \theta_{0,i}} = \mathbb{K}_m \left(\frac{\partial \theta_1}{\partial \theta_{0,i}} - 1 \right) - \frac{\partial \mathbb{P}(\theta_1)}{\partial \theta_{0,i}}$
$\frac{\partial C_2}{\partial K_i} = \frac{\partial \mathbb{K}_m}{\partial K_i} \Delta \theta_2 + \mathbb{K} \frac{\partial \Delta \theta_2}{\partial K_i} - \frac{\partial \mathbb{P}(\theta_2)}{\partial K_i}$	$\frac{\partial C_2}{\partial \theta_{0,i}} = \mathbb{K}_m \left(\frac{\partial \theta_2}{\partial \theta_{0,i}} - 1 \right) - \frac{\partial \mathbb{P}(\theta_2)}{\partial \theta_{0,i}}$
$\frac{\partial C_3}{\partial K_i} = \begin{pmatrix} 0 \\ \sum_{j=1}^N L_j \cos \theta_{1,j} \frac{\partial \theta_{1,j}}{\partial K_i} \\ \sum_{j=1}^N L_j \cos \theta_{2,j} \frac{\partial \theta_{2,j}}{\partial K_i} \end{pmatrix}$	$\frac{\partial C_3}{\partial \theta_{0,i}} = \begin{pmatrix} \sum_{j=1}^N L_j \cos \theta_{0,j} \\ \sum_{j=1}^N L_j \cos \theta_{1,j} \frac{\partial \theta_{1,j}}{\partial \theta_{0,i}} \\ \sum_{j=1}^N L_j \cos \theta_{2,j} \frac{\partial \theta_{2,j}}{\partial \theta_{0,i}} \end{pmatrix}$
$\frac{\partial C_4}{\partial K_i} = - \sum_{j=1}^N L_j \sin \theta_{2,j} \frac{\partial \theta_{2,j}}{\partial K_i}$	$\frac{\partial C_4}{\partial \theta_{0,i}} = - \sum_{j=1}^N L_j \sin \theta_{2,j} \frac{\partial \theta_{2,j}}{\partial \theta_{0,i}} + L_i \sin \theta_{0,i}$

Combining all the terms of the gradient due to K_i , we get the following,

$$\frac{\partial \mathcal{L}}{\partial K_i} = \frac{\partial \mathcal{J}}{\partial K_i} + \Lambda_1^T \frac{\partial \mathbb{K}_m}{\partial K_i} \Delta \theta_1 + \Lambda_2^T \frac{\partial \mathbb{K}_m}{\partial K_i} \Delta \theta_2 + \sum_{j=1}^N \left(\frac{\partial \mathcal{J}}{\partial \theta_{1,j}} + \Lambda_1^T \mathfrak{f}_1 + \Lambda_{3,2} L_j \cos \theta_{1,j} \right) \frac{\partial \theta_{1,j}}{\partial K_i}$$

$$+ \sum_{j=1}^N \left(\Lambda_2^T \mathfrak{f}_2 + \Lambda_{3,3} L_j \cos \theta_{2,j} + \Lambda_4 L_j \sin \theta_{2,j} \right) \frac{\partial \theta_{2,j}}{\partial K_i}$$

where,

$$\mathfrak{f}_1 = - \begin{bmatrix} \circ \\ \circ \\ \sum_{j=k}^{N+1} P_{Y,j} L_k \sin \theta_{1,k} \frac{\partial \theta_{1,k}}{\partial K_i} \\ \circ \\ \circ \end{bmatrix}$$

$$\mathcal{G}_2 = - \begin{bmatrix} \circ \\ \circ \\ \sum_{j=k}^{N+1} L_k (P_{Y,j} \sin \theta_{2,k} + P_{X,j} \cos \theta_{2,k}) \frac{\partial \theta_{2,k}}{\partial K_i} \\ \circ \\ \circ \end{bmatrix}$$

Similarly, combining all the terms of the gradient with respect to the initial orientation we get the following,

$$\begin{aligned} \frac{\partial \mathcal{L}}{\partial \theta_{0,i}} &= \frac{\partial J}{\partial \theta_{0,i}} + \sum_{j=1}^N \left(\frac{\partial J}{\partial \theta_{1,j}} + \Lambda_1^T \mathcal{G}_1 + \Lambda_{3,2} L_j \cos \theta_{1,j} \right) \frac{\partial \theta_{1,j}}{\partial \theta_{0,i}} \\ &\quad + \sum_{j=1}^N \left(\Lambda_2^T \mathcal{G}_2 + \Lambda_{3,3} L_j \cos \theta_{2,j} + \Lambda_4 L_j \sin \theta_{2,j} \right) \frac{\partial \theta_{2,j}}{\partial \theta_{0,i}} \end{aligned}$$

where,

$$\mathcal{G}_1 = - \begin{bmatrix} \circ \\ \circ \\ \sum_{j=k}^{N+1} P_{Y,j} L_k \sin \theta_{1,k} \frac{\partial \theta_{1,k}}{\partial \theta_{0,i}} \\ \circ \\ \circ \end{bmatrix}$$

$$\mathcal{G}_2 = - \begin{bmatrix} \circ \\ \circ \\ \sum_{j=k}^{N+1} L_k (P_{Y,j} \sin \theta_{2,k} + P_{X,j} \cos \theta_{2,k}) \frac{\partial \theta_{2,k}}{\partial \theta_{0,i}} \\ \circ \\ \circ \end{bmatrix}$$

The above equations provide the optimal solution for the problem when the gradients of the gradient of the Lagrangian reaches 0. We choose the values of Λ in such a way that eliminates our requirement to calculate $\frac{\partial \theta_{1,j}}{\partial K_i}$ and $\frac{\partial \theta_{1,j}}{\partial \theta_{0,i}}$.

Using a similar procedure, we can obtain the gradients for equation (35).

References

- Akagi, R., Y. Takai, M. Ohta, H. Kanehisa, Y. Kawakami, and T. Fukunaga. 2009. Muscle volume compared to cross-sectional area is more appropriate for evaluating muscle strength in young and elderly individuals. *Age and ageing* 38 (5):564–69. doi:[10.1093/ageing/afp122](https://doi.org/10.1093/ageing/afp122).
- Alexander, R. M. 1988. Why mammals gallop. *American zoologist* 28 (1):237–45. doi:[10.1093/icb/28.1.237](https://doi.org/10.1093/icb/28.1.237).
- Cao, Q., and I. Poulakakis. 2012. Passive quadrupedal bounding with a segmented flexible torso. *IEEE/RSJ International Conference on Intelligent Robots and Systems*, Vilamoura, 2012, pp. 2484–2489. doi:[10.1109/IROS.2012.6386183](https://doi.org/10.1109/IROS.2012.6386183).
- Chirikjian, G. S., and J. W. Burdick. 1994. A hyper-redundant manipulator. *IEEE Robotics and*

- Automation Magazine* 1 (4):22–29. doi:[10.1109/100.388263](https://doi.org/10.1109/100.388263).
- Christophy, M., M. Curtin, N. A. F. Senan, J. C. Lotz, and O. M. O'Reilly. 2013. On the modeling of the intervertebral joint in multibody models for the spine. *Multibody System Dynamics* 30 (4):413–32. doi:[10.1007/s11044-012-9331-x](https://doi.org/10.1007/s11044-012-9331-x).
- Conkur, E. S., and R. Buckingham. 1997. Clarifying the definition of redundancy as used in robotics. *Robotica* 15 (05): 583–86. doi:[10.1017/s0263574797000672](https://doi.org/10.1017/s0263574797000672).
- Culha, U. 2012. An actuated flexible spinal mechanism for a bounding quadrupedal robot. Doctoral dissertation, Bilkent University.
- Deb, K. 1999. An introduction to genetic algorithms. *Sadhana* 24 (4–5):293–315. doi:[10.1007/bf02823145](https://doi.org/10.1007/bf02823145).
- Ghosal, A. 2006. *Robotics: Fundamental Concepts and Analysis*. Oxford University Press, New Delhi.
- Haftka, R. T., and Z. Gurdal. 2012. *Elements of Structural Optimization*. vol. 11. Springer Science & Business Media, Dordrecht doi:[10.1007/978-94-011-2550-5](https://doi.org/10.1007/978-94-011-2550-5).
- Hutter, M., C. Gehring, D. Jud, A. Lauber, C. D. Bellicoso, V. Tsounis, and R. Diethelm. 2016. Anymal—a highly mobile and dynamic quadrupedal robot. IEEE/RSJ International Conference on Intelligent Robots and Systems (IROS), Daejeon, 2016, pp. 38–44. doi:[10.1109/IROS.2016.7758092](https://doi.org/10.1109/IROS.2016.7758092).
- Ijspeert, A. J., A. Crespi, D. Ryczko, and J.-M. Cabelguen. 2007. From swimming to walking with a salamander robot driven by a spinal cord model. *Science* 315 (5817):1416–20. doi:[10.1126/science.1138353](https://doi.org/10.1126/science.1138353).
- Khoramshahi, M., A. Spröwitz, A. Tuleu, M. N. Ahmadabadi, and A. J. Ijspeert. (2013a). Benefits of an active spine supported bounding locomotion with a small compliant quadruped robot. IEEE international conference on robotics and automation (ICRA), Karlsruhe, 2013, IEEE, pp. 3329–3334. doi:[10.1109/ICRA.2013.6631041](https://doi.org/10.1109/ICRA.2013.6631041).
- Khoramshahi, M., H. J. Bidgoly, S. Shafiee, A. Asaei, A. J. Ijspeert, and M. N. Ahmadabadi. (2013b). Piecewise linear spine for speed–energy efficiency trade-off in quadruped robots. *Robotics and Autonomous Systems* 61 (12):1350–59. doi:[10.1016/j.robot.2013.08.001](https://doi.org/10.1016/j.robot.2013.08.001).
- Lavaste, F., W. Skalli, S. Robin, R. Roy-Camille, and C. Mazel. 1992. Three-dimensional geometrical and mechanical modelling of the lumbar spine. *Journal of Biomechanics* 25 (10):1153–64. doi:[10.1016/0021-9290\(92\)90071-8](https://doi.org/10.1016/0021-9290(92)90071-8).
- Lei, J., H. Yu, and T. Wang. 2016. Dynamic bending of bionic flexible body driven by pneumatic artificial muscles (PAMs) for spinning gait of quadruped robot. *Chinese Journal of Mechanical Engineering* 29 (1):11–20. doi:[10.3901/cjme.2015.1016.123](https://doi.org/10.3901/cjme.2015.1016.123).
- MATLAB. 2012. *Natick, Massachusetts, Natick, Massachusetts, 7.12.0 (R2011a)*. The MathWorks Inc. Natick, Massachusetts.
- Raibert, M., K. Blankespoor, G. Nelson, and R. Playter. 2008. Bigdog, the rough-terrain quadruped robot. *IFAC Proceedings Volumes* 41 (2):10822–25. doi:[10.3182/20080706-5-kr-1001.01833](https://doi.org/10.3182/20080706-5-kr-1001.01833).
- Roos, L., F. Guenter, A. Guignard, and A. G. Billard. 2006. Design of a biomimetic spine for the humanoid robot robota. The first IEEE/RAS-EMBS international conference on biomedical robotics and biomechatronics, 2006, BioRob 2006, Pisa, 2006, pp. 329–334. doi:[10.1109/BIOROB.2006.1639108](https://doi.org/10.1109/BIOROB.2006.1639108).
- Sanchis-Moysi, J., F. Idoate, C. Dorado, S. Alayon, and J. A. Calbet. 2010. Large asymmetric hypertrophy of rectus abdominis muscle in professional tennis players. *PLoS One* 5 (12): e15858. doi:[10.1371/journal.pone.0015858](https://doi.org/10.1371/journal.pone.0015858).

- Seifried, R. 2014. *Dynamics of Underactuated Multibody Systems*. Berlin: Springer.
- Semini, C., N. G. Tsagarakis, E. Guglielmino, M. Focchi, F. Cannella, and D. G. Caldwell. (2011). Design of HyQ—a hydraulically and electrically actuated quadruped robot. *Proceedings of the Institution of Mechanical Engineers, Part I: Journal of Systems and Control Engineering* 225 (6):831–49. doi:[10.1177/0959651811402275](https://doi.org/10.1177/0959651811402275).
- Seok, S., A. Wang, M. Y. Chuah, D. Otten, J. Lang, and S. Kim. 2013. Design principles for highly efficient quadrupeds and implementation on the MIT Cheetah robot. IEEE international conference on robotics and automation (ICRA), Karlsruhe, 2013, IEEE, pp. 3307–3312. doi:[10.1109/ICRA.2013.6631038](https://doi.org/10.1109/ICRA.2013.6631038)
- Xu, D., and G. Ananthasuresh. 2003. Freeform skeletal shape optimization of compliant mechanisms. *Journal of Mechanical Design* 125 (2):253–61. doi:[10.1115/1.1563634](https://doi.org/10.1115/1.1563634).
- Zhou, H., and K.-L. Ting. 2008. Geometric modeling and optimization of multimaterial compliant mechanisms using multilayer wide curves. *Journal of Mechanical Design* 130 (6):062303. doi:[10.1115/1.2902278](https://doi.org/10.1115/1.2902278)